Sensitivity Enhancement and Heteronuclear Distance Measurements in Biological ^{17}O Solid-State NMR

Andreas Brinkmann* and Arno P. M. Kentgens

Physical Chemistry/Solid State NMR, Institute for Molecules and Materials, Radboud University Nijmegen, Toernooiveld 1, 6525 ED Nijmegen, The Netherlands

Received: May 8, 2006; In Final Form: June 16, 2006

In this contribution we present a comprehensive approach to study hydrogen bonding in biological and biomimetic systems through ^{17}O and $^{17}O-^{1}H$ solid-state NMR combined with density functional theory calculations of ^{17}O and ^{1}H NMR parameters. We explore the signal enhancement of ^{17}O in L-tyrosine·HCl using repetitive double-frequency swept radio frequency pulses in solid-state NMR. The technique is compatible with high magnetic fields and fast magic-angle spinning of the sample. A maximum enhancement by a factor of 4.3 is obtained in the signal-to-noise ratio of the selectively excited ^{17}O central transition in a powdered sample of $^{17}O^{\eta}$-L-tyrosine·HCl at an external field of 14.1 T and a spinning frequency of 25 kHz. As little as 128 transients lead to meaningful ^{17}O spectra of the same sample at an external field of 18.8 T and a spinning frequency of 50 kHz. Furthermore we employed supercycled symmetry-based pulse sequences on the protons to achieve heteronuclear longitudinal two-spin-order (I_zS_z) recoupling to determine $^{17}O-^{1}H$ distances. These sequences recouple the heteronuclear dipolar $^{17}O-^{1}H$ couplings, where dipolar truncation is absent, while decoupling the homonuclear proton dipolar interactions. They can be applied at fast magic-angle-spinning frequencies up and beyond 50 kHz and are very robust with respect to ^{17}O quadrupolar couplings and both ^{17}O and ^{1}H chemical shift anisotropies, which makes them suitable for the use at high external magnetic fields. The method is demonstrated by determining the $^{17}O^{\eta}-^{1}H$ distance in L-tyrosine·HCl at a spinning frequency of 50 kHz and an external field of 18.8 T.

1. Introduction

Hydrogen bonding is an essential component of the structure and function of biological molecules.[1,2] Hydrogen bonds are difficult to quantify by X-ray crystallography because of the low scattering cross section of hydrogen atoms. Although neutron diffraction does not suffer from this limitation, it requires suitable crystals of sufficient size, which can be difficult or impossible to obtain. In addition, most biological materials are inherently disordered. As a result, solid-state nuclear magnetic resonance (NMR) is an ideal tool to study these materials. Solid-state NMR spectroscopy of ^{17}O is a powerful tool to study hydrogen bonds since the ^{17}O chemical shift and quadrupolar coupling are claimed to be very sensitive to the strength and geometry of the hydrogen bonds. In recent years, several groups have demonstrated the feasibility of ^{17}O NMR experiments in small organic molecules,[3−6] nucleic acid basis,[7] amino acids,[3,6,8−10] polypeptides,[11,12] and proteins,[13,14] showing a correlation between hydrogen bonding and ^{17}O chemical shifts and quadrupolar couplings.

^{17}O is a quadrupolar nucleus ($S = {}^{5}/_{2}$) with a low sensitivity and a low natural abundance. The last difficulty can be overcome by isotopic labeling of the samples, but due to the low gyromagnetic ratio, γ sensitivity remains an issue. In this respect important steps in the design of solid-state NMR experiments have been made to enhance the sensitivity of half-integer quadrupolar nuclei by transferring population from the satellite transitions to the central transition, prior to applying a central-transition selective 90° pulse followed by signal detection. In general this transfer is achieved by adiabatically inverting the satellite transitions using amplitude modulated radio frequency (rf) pulses.[15−19] It has been demonstrated that the concept of double-frequency sweeps (DFS) can be favorably combined with magic-angle spinning (MAS) of the sample as the combined effect of sample rotation and an amplitude-modulated frequency sweep allows adjustment in the adiabaticity of the inversion of the satellite transitions.[20,21] In powered samples, both under static and MAS conditions, a random distribution of enhancement factors in the range 1 to 2*S* over all molecular orientations in the powder is achieved and the original quadrupolar powder line shape is preserved.[21] The original implementation of DFS uses frequency sweeps, in which the frequency of the amplitude modulation depends linearly on time (linear sweeps). Siegel et al. have demonstrated that hyperbolic secant DFS leads to improved signal enhancements.[22,23] In this case the amplitude of the rf pulse is modulated according to a hyperbolic secant function, while the rf frequency follows a hyperbolic tangent function with a limited frequency bandwidth.

Recently, it has been shown that in powdered samples the population transfer pulse scheme followed by a central-transition selective 90° pulse and signal detection may be repeated several times prior to letting the spin-system relax to thermal equilibrium during the recovery time interval.[24,25] In the case of "multiple rotor assisted population transfer (multiple RAPT)",[24] an enhancement in the signal-to-noise ratio by a factor of 2.3 (determined from Figure 2 in ref 24) was obtained for ^{27}Al ($S = {}^{5}/_{2}$) in albite under MAS condition. Application of the repetitive DFS (rDFS) scheme[25] under double rotation (DOR)

* To whom correspondence may be addressed. Fax: +31-24-3652112, E-mail: A.Brinkmann@science.ru.nl.

10.1021/jp062809p CCC: $33.50
Published on Web 07/27/2006

condition leads to an enhancement by a factor of 2.9 in the signal-to-noise (*S*/*N*) ratio for ^{27}Al in albite. Similar enhancement factors were obtained under MAS condition (results not shown). In this contribution we will show that the rDFS significantly enhances the *S*/*N* ratio in ^{17}O MAS NMR, by demonstrating it on the isotopically labeled amino acid L-tyrosine·HCl.

Despite the ^{1}H chemical shift, the ^{17}O chemical shift, and quadrupolar coupling being sensitive to hydrogen bonding, measuring the internuclear ^{17}O−^{1}H distance is the most direct and accurate way to characterize the hydrogen bond, however. Van Eck and Smith determined the ^{17}O−^{1}H heteronuclear dipolar coupling in a static powder of $Mg(OH)_2$ by letting ^{17}O central transition single-quantum coherence evolve for a defined time interval without proton decoupling during a spin-echo experiment.[26] As a consequence the ^{17}O single quantum coherence evolved in the presence of the ^{17}O−^{1}H heteronuclear dipolar coupling. The ^{1}H−^{1}H homonuclear dipolar couplings were removed by Lee−Goldburg decoupling[27] of the protons during the evolution time.

Although MAS is an essential component of many realistic applications of solid-state NMR, the effect of the heteronuclear dipolar couplings containing distance information is strongly attenuated by the MAS. As a result the estimation of internuclear distances requires the employment of recoupling pulse sequences, to suspend the averaging effect of the MAS over a defined time interval. There are many different types of pulse sequences achieving recoupling of heteronuclear dipolar couplings.[28−30] A detailed overview of the different properties of a selection of heteronuclear recoupling sequences can be found in ref 31. In the following, the most prominent sequences are briefly presented and discussed in the context of estimating ^{17}O−^{1}H heteronuclear dipolar couplings. The two spin species are denoted *S* and *I*, where *S* represents the heteronuclei, in particular half-integer quadrupolar nuclei, and *I* represents the protons.

In Hartmann−Hahn cross polarization (HH-CP) under MAS,[32] resonant rf irradiation is applied to both spin species *I* and *S* to achieve heteronuclear recoupling. It is widely employed in static and rotating solids to enhance signals from heteronuclei with low gyromagnetic ratios by transferring magnetization from the abundant protons. Cross-polarization involving quadrupolar nuclei is a complicated process because of the difficulty to spin lock the central transition transverse magnetization.[33] Although Mali and Kaučič demonstrated that ^{27}Al−^{1}H distances in aluminophosphate molecular sieves can be determined by HH-CP dynamics,[34] HH-CP involving quadrupolar nuclei is not generally applicable to determine internuclear distances.

Popular pulse schemes for heteronuclear recoupling in MAS NMR between a spin-$^1/_2$ and a half-integer quadrupolar nucleus are the REDOR,[35,36] and the related TEDOR,[37] REAPDOR,[36,38,39] and TRAPDOR[40] pulse sequences. The REDOR sequence is only applied to the *I*-spins and accomplishes *longitudinal two-spin-order* (I_zS_z) recoupling of the heteronuclear dipolar interactions between *S* and *I*-spins in first order. One advantage of REDOR is that the recoupled heteronuclear dipolar interactions commute for different spin pairs. The evolution of the heteronuclear spin system can be described as a superposition of the evolution of isolated spin pairs. Noncommuting dipolar interactions on the other hand lead to "dipolar truncation";[41] i.e., the measurement of a weak dipolar coupling between two spins is prevented if one or both spins are also strongly dipolar coupled to other spins. REDOR does not suffer from dipolar truncation. REDOR recouples simultaneously the chemical shift anisotropies of the *I*-spins in first order, but they commute with the heteronuclear dipolar interactions. Thus in practice the estimation of heteronuclear distances is hardly influenced by *I*-spin CSA interactions. REDOR has been successfully combined with multiple-quantum magic-angle spinning (MQMAS)[42] to achieve high-resolution ^{27}Al spectra in combination with determining ^{19}F−^{27}Al internuclear distances.[43,44] The group of Spiess used rotor-encoded spectroscopy[45] employing the REDOR sequence to determine ^{23}Na−^{1}H distances in an MQMAS experiment.[46] REDOR also recouples the *I*-spin homonuclear dipolar couplings in first order, where the size of the recoupled terms depends on the ratio of the duration of the 180° pulses with respect to the period of the sample rotation. Hence, only in the limit of short pulses with respect to the rotation period, homonuclear *I*-spin decoupling is achieved, while under fast MAS condition and the usual rf field limitations for conventional MAS probes, substantial recoupling of the *I*-spin homonuclear dipolar interactions occurs. As a consequence, REDOR is not the ideal choice to estimate internuclear distances between heteronuclei and protons in proton-rich samples.

During recent years symmetry theory has been established as a powerful tool in the design of rotor-synchronized rf pulse sequences that selectively preserve and restore certain spin interactions while suppressing others.[30] Pulse sequences denoted $R18_1^7$ and $R18_2^5$ have been described, which are applied to the *I*-spins and accomplish *single-quantum* recoupling of the heteronuclear dipolar interactions while suppressing the *I*-spin homonuclear dipolar couplings.[47−49] These sequences lead to strong dipolar oscillations in powdered samples and have been successfully used to detect perturbations of ^{15}N−^{1}H bond lengths caused by intermolecular hydrogen bonds.[49] Van Beek et al. applied the $R18_2^5$ sequence to determine ^{17}O−^{1}H distances and the relative orientation of the ^{17}O quadrupolar tensor and the ^{17}O−^{1}H dipolar coupling in powdered samples of isotopically labeled $Mg(OH)_2$ and glycine·HCl.[50] However, in the case of single-quantum heteronuclear recoupling, the recoupled heteronuclear dipolar interactions do not commute for different spin pairs. Hence these sequences suffer from dipolar truncation. Furthermore, the terms of the simultaneously recoupled CSA of the irradiated *I*-spins do not commute with the heteronuclear dipolar coupling terms. This may not always be desirable, since the ^{1}H CSA in carboxyl and hydroxyl groups can be in the order of 20 ppm, hence influencing the ^{17}O−^{1}H distance determination, especially in large external magnetic fields. Therefore, in this contribution we choose another class of symmetry-based RN_n^ν pulse sequences to determine ^{17}O−^{1}H distances. These sequences achieve heteronuclear longitudinal two-spin-order (I_zS_z) recoupling, hence not suffering from dipolar truncation, while decoupling the *I*-spin homonuclear dipolar couplings.[31,30] The heteronuclear longitudinal two-spin-order recoupling sequences are demonstrated by numerical simulations and by experimentally estimating the $^{17}O^{\eta}$−$^{1}H^{\eta}$ distance in the hydroxyl group of isotopically labeled $^{17}O^{\eta}$-L-tyrosine·HCl.

Quantum chemical calculations have become increasingly important to assist the interpretation of experimental NMR data and to provide supplementary information. Gervais et al. have recently calculated the ^{17}O chemical shift and quadrupolar tensors for the crystalline form of different amino acids by density functional theory (DFT) under periodic boundary conditions.[51] For this contribution we calculated ^{1}H CSA tensors, ^{17}O CSA tensors, and quadrupolar coupling tensors in L-tyrosine·HCl using the commercially available Amsterdam Density Functional (ADF) package.[52−54] Our results for ^{17}O will be compared to those in ref 51.

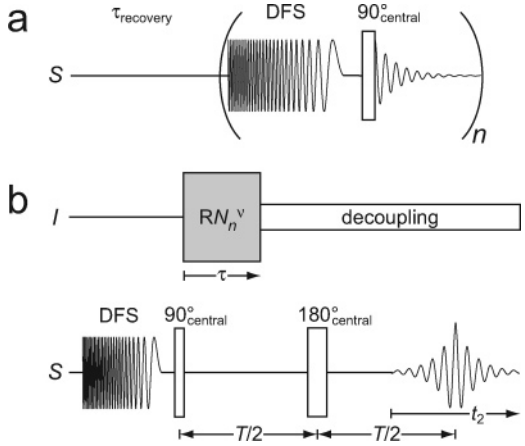

Figure 1. (a) Radio frequency pulse sequence for the repetitive DFS experiment on the half-integer spin species *S*. The subscript "central" denotes a central transition selective pulse with the given rotation angle and phase (i.e., $\omega_1 \ll \omega_Q$). (b) Sequence for determining heteronuclear dipolar couplings between the spin-$^1/_2$ species *I* and the half-integer spin species *S*.

In this contribution we combine the approaches described above to develop a comprehensive methodology to study hydrogen bonding in biological systems through ^{17}O and ^{17}O−^{1}H NMR.

2. Enhancement in the Central-Transition Population Difference by Double Frequency Sweeps

The pulse sequence for the rDFS experiment is shown in Figure 1a. The row marked *S* denotes the rf fields at the Larmor frequency of the half-integer quadrupolar nucleus, in our case ^{17}O. The pulse sequence starts with the recovery time interval during which the spin system is allowed to relax into thermal equilibrium. The following pulse sequence block is repeated *n* times: it consists of a DFS prior to a selective 90° pulse on the *S*-spin central transition (rf field strength ω_1 small compared to the quadrupolar frequency ω_Q) followed by detection of the complex NMR *S*-spin signal.

Consider the general case of a half-integer spin $S > {}^1/_2$ nuclei. An optimized DFS ideally inverts the satellite transitions adiabatically, leading to an enhancement of 2*S* in the central transition population difference for a single molecular orientation. The population difference in the central transition is converted into observable single-quantum (1Q) coherence by the following central-transition selective 90° pulse. The central-transition 1Q coherence is subject to T_2 relaxation during the subsequent signal detection. However, there still exist population differences in the satellite transitions. The situation for $S = {}^5/_2$ and $\gamma < 0$ (as for ^{17}O) is depicted in Figure 2. Therefore, the sequence consisting of the DFS followed by a central-transition selective 90° pulse and signal detection may be repeated prior to letting the spin-system relax to thermal equilibrium during the recovery time interval.[25] If s^0 denotes the signal intensity in the free induction decay (FID) for a single molecular orientation detected after a central-transition selective 90° pulse is applied to the equilibrium central transition populations, the signal intensities for the *k*th repetition in an ideal rDFS experiment are given by

$$s_k = 2(S-k)s^0 \quad \text{with} \quad k = 0, 1, ..., S - \frac{1}{2} \qquad (1)$$

For example, in the case of $S = {}^5/_2$ this corresponds to signal enhancement factors of 5, 3, and 1, as shown in Figure 2. The individual FIDs may be summed, where optimal enhancement in the *S*/*N* ratio is achieved by weighting each FID with its own intensity.[24] This corresponds to a matched filter. If σ^0 denotes the root-mean-square noise in a single transient, the *S*/*N* ratio for the weighted sum is given by

$$(S/N)_{\text{weighted}} = \frac{s^0}{\sigma^0}\sqrt{\frac{2}{3}S(S+1)(2S+1)} \qquad (2)$$

The maximum theoretical enhancement in the *S*/*N* ratio that can be achieved with rDFS for a single molecular orientation is given by 5.92 for $S = {}^5/_2$.

In realistic powdered samples spinning at the magic angle, a single DFS achieves a randomly distributed enhancement in the range 1 to 2*S* for various molecular orientations.[21] Therefore rDFS is beneficial for powdered samples as well. Because of the noncomplete inversion of the satellite transitions in each DFS step, the individual enhancements are on one hand smaller, but on the other hand the process may be repeated more often before the satellite transitions are depleted. The signal intensities in the consecutive FIDs decay approximately exponentially in powdered samples. Assuming a gain of *G* for the FID after the first DFS and an exponential decay of e^{-x} in signal intensity between consecutive FIDs the *S*/*N* ratio for the weighted sum of the individual FIDs can be maximally improved by a factor of (ref 25)

$$(\langle S/N\rangle_{\text{powder}})_{\text{weighted}} = \frac{s^0}{\sigma^0} G\sqrt{1/(1-e^{-2x})} \qquad (3)$$

3. Symmetry-Based Heteronuclear Longitudinal Two-Spin-Order Dipolar Recoupling

In the following we discuss the properties of the class of rotor-synchronized RN_n^ν pulse sequences that accomplish heteronuclear longitudinal two-spin-order recoupling while decoupling homonuclear dipolar interactions. We employ these sequences to estimate ^{17}O−^{1}H distances using the pulse scheme shown in Figure 1b. The row marked *I* denotes rf fields at the Larmor frequency of the abundant protons, while the row marked *S* denotes the rf fields at the ^{17}O Larmor frequency. The pulse scheme is based on the dipolar and chemical shift (DIPSHIFT) correlation experiment.[55] First the central transition population of the ^{17}O is enhanced by a DFS followed by a selective 90° pulse on the ^{17}O central transition. The resulting central transition transverse magnetization is subjected to a Hahn echo[56] sequence of total duration *T* and a central transition selective 180° pulse as refocusing pulse in the center of the evolution time interval. For a time τ the ^{17}O central transition transverse magnetization evolves in the presence of a RN_n^ν heteronuclear recoupling sequence on the protons. For the remaining time of the Hahn echo proton decoupling is applied. The complete ^{17}O spin-echo is detected during the time interval t_2.

3.1. Pulse Sequence Symmetries and Supercycles. The symmetry-based RN_n^ν recoupling sequences, possible supercycles, and the theory of these schemes in first- and second-order average Hamiltonians have been discussed in great detail before.[30,31,47,57−61] Here we will briefly summarize the main results in view of our application. For simplicity consider a spin system consisting of a single half-integer quadrupolar *S*-spin and several spin-$^1/_2$ *I*-spins. The RN_n^ν sequence is solely applied to the *I*-spins and defined by the set of three integer symmetry numbers (N, n, ν), where N is even. It is constructed from a basic pulse element $\mathcal{R}$ of duration $\tau_R = n\tau_r/N$, where $\tau_r = 2\pi/\omega_r$ is the rotational period and ω_r the angular spinning

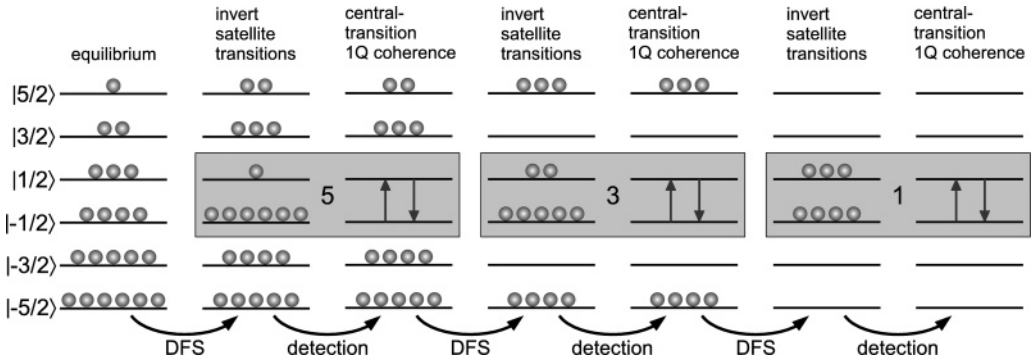

Figure 2. Schematic energy level diagram for a spin-$^5/_2$ nucleus ($\gamma < 0$). The pictorial representation of populations and coherences[89] is shown for a repeated scheme consisting of satellite transition population inversion followed by conversion to detectable central transition single-quantum coherence. The enhancement of the central transition population difference by factors of 5, 3, and 1 is indicated.

frequency. If all interactions other than that with the rf field are ignored, the inversion element $\mathscr{R}$ effects a net rotation of π of the *I*-spins around the *x*-axis in the rotating frame. A second element $\mathscr{R}'$ is derived from $\mathscr{R}$ by reversing the sign of all rf phases. The $\mathrm{R}N_n^\nu$ sequence is formed by repeating the pair $(\mathscr{R})_\phi(\mathscr{R}')_{-\phi}$ $N/2$ times, where the additional phase shift is given by $\phi = \pi\nu/N$. The duration of the whole $\mathrm{R}N_n^\nu$ sequence is given by $n\tau_\mathrm{r}$.

The nuclear spin interactions of the *I*-spins may be classified in terms of their properties under rotations by the quantum numbers $\{l, m, \lambda, \mu\}$, where $\{l, m\}$ denote the rank and component with respect to spatial rotations of the sample and $\{\lambda, \mu\}$ denote the rank and component with respect to *I*-spin rotations. For example the homonuclear dipolar interaction between *I*-spins has ranks $l = 2$, $\lambda = 2$; the homonuclear isotropic *J*-coupling between *I*-spins has ranks $l = 0$, and $\lambda = 0$; the chemical shift anisotropy of the *I*-spins and the heteronuclear dipolar interaction between *S* and *I*-spins have both ranks $l = 2$, $\lambda = 1$; the isotropic chemical shift of the *I*-spins and the heteronuclear isotropic *J*-coupling between *S* and *I*-spins have ranks $l = 0$, $\lambda = 1$. Explicit expressions for the various terms may be found in ref 62.

The rotor-synchronized $\mathrm{R}N_n^\nu$ sequences may be analyzed using average Hamiltonian theory.[63] Selection rules can be derived, which predict if a certain interaction term with the quantum numbers $\{l, m, \lambda, \mu\}$ is present (symmetry-allowed) in the first-order average Hamiltonian under a pulse sequence with the set of symmetry numbers (N, n, ν) (refs 30, 31, 47, and 61). These selection rules may be used to design pulse sequences which provide heteronuclear longitudinal two-spin-order dipolar recoupling and at the same time decouple the homonuclear *I*-spin dipolar interactions. Suitable symmetries have been presented before in refs 30 and 31 and include $\mathrm{R}12_3^1$, $\mathrm{R}12_3^2$, $\mathrm{R}12_3^4$, $\mathrm{R}12_3^5$, $\mathrm{R}16_4^1$, $\mathrm{R}16_4^3$, $\mathrm{R}16_4^5$, $\mathrm{R}16_4^7$, etc. These symmetries have the following properties:

(i) Terms with $\{l, m, \lambda, \mu\} = \{2, \pm2, 1, 0\}$ are symmetry-allowed in the first-order average Hamiltonian. That corresponds to selective recoupling of the *IS* heteronuclear dipolar coupling interactions and the *I*-spin chemical shift anisotropies.

(ii) Since the spin-component $\mu = 0$ is associated with the two spatial components $m = \pm2$, the resulting average Hamiltonian is not *γ-encoded*.[64] A pulse sequence is called γ-encoded if the induced modulation of the NMR signal for a single molecular orientation depends only on two of the three Euler angles describing the relative orientation of a molecular fixed reference frame with respect to a sample holder reference frame. On one hand the lack of γ-encoding reduces the amplitude of dipolar oscillations in powdered samples, which makes quantitative distance measurements more difficult. On the other hand non-γ-encoded sequences are generally more robust and superior for long-range distance estimations.[65−67]

(iii) The recoupled terms of the *IS* heteronuclear dipolar interactions commute for different spin pairs.

(iv) The recoupled terms of the *I*-spin CSA interactions and the heteronuclear dipolar couplings between *S* and *I*-spins commute. As a consequence the oscillations of the *S*-spin signal due to the heteronuclear dipolar couplings are not sensitive to the *I*-spin chemical shift anisotropies. This allows the determination of the heteronuclear dipolar couplings without any knowledge (size and orientation) of the *I*-spin CSA interactions.

(v) Second-order cross terms between the *S*-spin quadrupolar coupling and the *IS* heteronuclear dipolar coupling with $\{l, m, \lambda, \mu\} = \{2, \pm2, 1, 0\}$ and $\{4, \pm2, 1, 0\}$ are symmetry allowed in first-order average Hamiltonian theory and are therefore recoupled. However, these terms are scaled by the ratio of the *S*-spin quadrupolar frequency and the *S*-spin Larmor frequency with respect to the *IS* heteronuclear dipolar coupling interactions. In the case considered in this paper ($S = {}^{17}\mathrm{O}$, quadrupolar coupling constants C_Q up to 10 MHz [quadrupolar frequencies up to 1.5 MHz], and a static field of 18.8 T [Larmor frequency 108.5 MHz]) this ratio is in the order of 1−1.5% and therefore we will not include these terms in the further discussion. It should be noted that these terms may play a more important role in other systems, e.g., in the case of $^{14}\mathrm{N}$ ($S = 1$) in amino acids, polypeptides, and proteins at an external field of 7.05 T, this ratio can be on the order of 20%.

(vi) The *I*-spin homonuclear isotropic *J*-couplings have the symmetry numbers $\{l, m, \lambda, \mu\} = \{0, 0, 0, 0\}$ and are therefore symmetry-allowed under any $\mathrm{R}N_n^\nu$ sequence on the *I*-spins.

(vii) All terms of the homonuclear dipolar couplings between *I*-spins, isotropic chemical shifts of the *I*-spins, and isotropic heteronuclear *J*-couplings between *S* and *I*-spins are suppressed in the first-order average Hamiltonian.

In particular, the subset of the above symmetries of the type $\mathrm{R}(4n)_n^{2n-1}$ for integer n with $n > 2$ is interesting, since the phase shift between consecutive basic elements in the pulse sequence is given by $\pi - \pi/(2n)$, i.e., the larger the value of n, the closer to π is the phase shift. As a result adjacent pairs of basic elements have nearly opposite phases and combine to achieve an approximate internal compensation for rf field errors.[47] In the following, we investigated solutions of this type, which include the symmetries

$$\mathrm{R}(4n)_n^{2n-1} = \mathrm{R}12_3^5, \mathrm{R}16_4^7, \mathrm{R}20_5^9, \mathrm{R}24_6^{11}, \mathrm{R}28_7^{13}, \mathrm{R}32_8^{15}, \ldots \quad \text{for} \quad n = 2, 3, 4, \ldots \quad (4)$$

As a basic element we chose a single 180° pulse around the rotating-frame x-axis ($\mathscr{R} = 180_0$), spanning the entire period τ_R (windowless pulse). As a consequence all the above listed pulse sequence symmetries require the of the rf field strength on the I-spins to be twice the spinning frequency, $\omega_1^I/\omega_r = 2$, which makes these sequences ideal for application at very fast spinning frequencies around 50 kHz. Other possible choices for $\mathscr{R}$, especially for application at lower spinning frequencies, are composite pulses[68] or windowed elements.[69]

It has been shown before that the robustness of RN_n^ν sequences with respect to isotropic chemical shifts, chemical shift anisotropies, rf inhomogeneity, and instrumental errors in the rf phase setting can be further improved by supercycling.[60,61,65,67,70] We used a combination of inversion supercycles, in which all rf phases are inverted in adjacent pulse sequence blocks, and "multiple-quantum" (MQ) phase cycles, in which the overall rf phase of consecutive pulse sequence blocks is incremented.[59,61,65,67,70] The nested supercycles are denoted $(RN_n^\nu\ RN_n^{-\nu})M^1$ (ref 61), where in particular we implemented the following RN_n^ν sequences and supercycles

$$(R12_3^5\,R12_3^{-5})3^1 = [R12_3^5\,R12_3^{-5}]_0[R12_3^5\,R12_3^{-5}]_{120}[R12_3^5\,R12_3^{-5}]_{240} \quad (5)$$

$$(R32_8^{15}\,R32_8^{-15})2^1 = [R32_8^{15}\,R32_8^{-15}]_0[R32_8^{15}\,R32_8^{-15}]_{180} \quad (6)$$

$$(R32_8^{15}\,R32_8^{-15})3^1 = [R32_8^{15}\,R32_8^{-15}]_0[R32_8^{15}\,R32_8^{-15}]_{120}[R32_8^{15}\,R32_8^{-15}]_{240} \quad (7)$$

where the sequence $RN_n^{-\nu}$ is derived from RN_n^ν by reversing the sign of all rf phases. The notation $[...]_\phi$ indicates an overall phase shift in degrees of the bracketed sequence by ϕ. A detailed discussion of these supercycles and their theoretical treatment can be found in ref 61.

3.2. Average Hamiltonian. The symmetric pulse sequences discussed in the previous section provide a time-independent first-order average Hamiltonian of the form

$$\bar{H}^{(1)} = \bar{H}_S + \bar{H}_I^{(1)} + \bar{H}_{IS}^{(1)} \quad (8)$$

where the S-spin Hamiltonian is given by

$$\bar{H}_S = \Omega_0^S S_z + \bar{H}_Q^{(2)} \quad (9)$$

and Ω_0^S is the resonance offset of the S-spin and $\bar{H}_Q^{(2)}$ is the Hamiltonian of the second-order quadrupolar coupling averaged by MAS. The S-spin central transition is selectively excited and subjected to an Hahn echo during the pulse sequence shown in Figure 6. Hence, the first-order central-transition quadrupolar Hamiltonian $\bar{H}_Q^{(1)}$ is absent.

The first-order recoupled homonuclear I-spin and heteronuclear IS-spin average Hamiltonians are given by

$$\bar{H}_I^{(1)} = \sum_j \omega_j I_{jz} \quad (10)$$

$$\bar{H}_{IS}^{(1)} = \sum_j \omega_{jS} I_{jz} S_z \quad (11)$$

where the sums are taken over all I-spins. We have ignored all homonuclear isotropic J-couplings of the I-spins. The (real) frequency ω_j is the recoupled CSA of spin I_j and the (real) frequency ω_{jS} is the recoupled heteronuclear dipolar coupling between spins I_j and S. For all symmetries in eq 4 and the basic element $\mathscr{R} = 180_0$ these two frequencies are given by

$$\omega_\Lambda = \frac{1}{\sqrt{6}} \mathrm{Re}([A_{22}^\Lambda]^R \exp\{-2i(\alpha_{RL}^0 - \omega_r t_0)\}) \quad (12)$$

where $\Lambda = \{jS,j\}$ stands for the type of spin interactions: heteronuclear dipolar coupling and CSA, respectively. The starting time point of the recoupling sequence is given by t_0, and α_{RL}^0 denotes the initial position of the rotor at that time point. $[A_{22}^\Lambda]^R$ is the space component $m = 2$ of the interaction tensor Λ with rank $l = 2$, written in the rotor-fixed frame. The component in the rotor-fixed frame is obtained by transforming it from the principal axis system as follows:

$$[A_{22}^\Lambda]^R = \sum_{m,m'=-2}^{2} [A_{2m}^\Lambda]^P\, D_{mm'}^{(2)}(\Omega_{PM}^\Lambda) D_{m'2}^{(2)}(\Omega_{MR}) \quad (13)$$

The Euler angles $\Omega_{PM}^\Lambda = \{\alpha_{PM}^\Lambda, \beta_{PM}^\Lambda, \gamma_{PM}^\Lambda\}$ describe the relative orientation of the principal axis frame of the interaction Λ and a molecule-fixed frame. The Euler angles $\Omega_{MR} = \{\alpha_{MR},\beta_{MR},\gamma_{MR}\}$ relate the molecular frame to a frame fixed on the rotor and are random variables in a powder. In the case of the heteronuclear dipolar coupling between spins S and I_j, only the component $[A_{20}^{jS}]^P = 2b_{jS}$ is nonzero, where the dipolar coupling constant b_{jS} is related to the internuclear distance r_{jS} and the gyromagnetic ratios γ_S and γ_I by $b_{jS} = -(\mu_0/4\pi)\gamma_S\gamma_I\hbar r_{jS}^{-3}$. In the case of the CSA of spin I_j, only the components $[A_{20}^j]^P = -\gamma_j B_0\, \delta_{\mathrm{aniso}}^j$ and $[A_{2\pm2}^j]^P = -\eta_j[A_{20}^j]^P/\sqrt{6}$ are nonzero, where B_0 is the external static magnetic field, $\delta_{\mathrm{aniso}}^j = \delta_{33}^j - \delta_{\mathrm{iso}}^j$ is the anisotropic chemical deshielding constant, and $\eta_j = (\delta_{22}^j - \delta_{11}^j)/\delta_{\mathrm{aniso}}^j$ is the asymmetry parameter. The isotropic chemical shift is given by $\delta_{\mathrm{iso}}^j = (\delta_{11}^j + \delta_{22}^j + \delta_{33}^j)/3$, and δ_{11}^j, δ_{22}^j, and δ_{33}^j denote the principal values of the chemical shift tensor, labeled such that $|\delta_{33}^j - \delta_{\mathrm{iso}}^j| \geq |\delta_{11}^j - \delta_{\mathrm{iso}}^j| \geq |\delta_{22}^j - \delta_{\mathrm{iso}}^j|$.

For all symmetries given in eq 4, assuming the basic element $\mathscr{R} = 180_0$, the frequency of the heteronuclear dipolar interaction (eq 12) between spins S and I_j is given by

$$\omega_{jS} = \frac{2}{\sqrt{6}} b_{jS}\, \mathrm{Re}\Big(e^{i2(\omega_r t_0 - \alpha_{RL}{}^0 - \gamma_{MR})} \times \sum_{m=-2}^{2} d_{0m}^{(2)}(\beta_{PM}^{jS})\, d_{m2}^{(2)}(\beta_{MR})\, e^{-im(\gamma_{PM}^{jS} + \alpha_{MR})}\Big) \quad (14)$$

where the Euler angles $\Omega_{PM}^{jS} = \{\alpha_{PM}^{jS},\beta_{PM}^{jS},\gamma_{PM}^{jS}\}$ describe the transformation of each heteronuclear dipolar coupling from its principal axis system to a molecule fixed frame.

The heteronuclear dipolar coupling terms in eq 11 commute with each other for different spin pairs (I_j, S). Therefore, using the rf pulse scheme shown in Figure 6 with one of the symmetries given in eq 4 results in the S-spin-echo intensity

$$S(\tau) = \left\langle \prod_j \cos\left(\frac{1}{2}\omega_{jS}\tau\right)\right\rangle_{\Omega_{MR}} \quad (15)$$

where $\langle\cdots\rangle_{\Omega_{MR}}$ denotes the orientational average over all possible molecular orientations Ω_{MR} in the powder.

4. Details of the Experiments and Simulations

4.1. Sample. The solid-state NMR experiments were performed on a sample of [35−40% $^{17}O^\eta$]-L-tyrosine·HCl, for

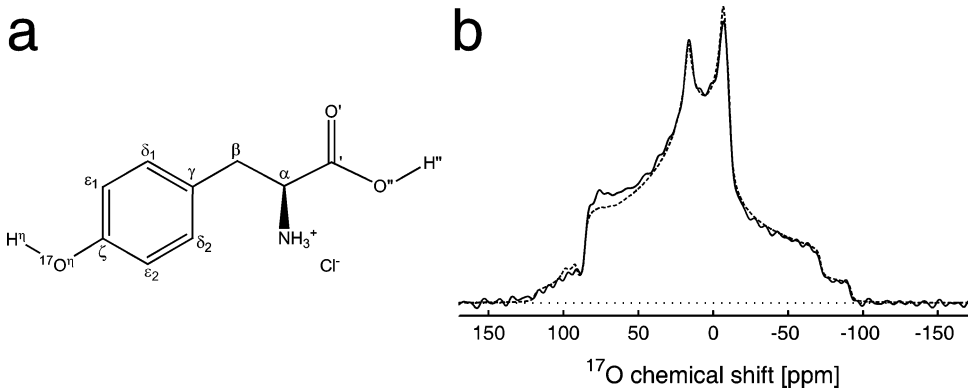

Figure 3. (a) Molecular structure of $^{17}O^{\eta}$-L-tyrosine·HCl. We use the nomenclature recommended by the IUPAC.[90] (b) Solid line: Experimental single-pulse ^{17}O spectrum of [35−40% $^{17}O^{\eta}$]-L-tyrosine·HCl obtained at a static field of 14.1 T and a spinning frequency of 25 kHz. Dashed line: Best fit simulated second-order quadrupolar line shape.

which the molecular structure is shown in Figure 3a. [35−40% $^{17}O^{\eta}$]-L-tyrosine was purchased from Cambridge Isotope Laboratories and recrystallized from a 9 M solution of HCl in water by slow evaporation of the solvent at room temperature.

4.2. Solid-State NMR. All experiments were performed at static magnetic fields of 14.1 and 18.8 T using a Varian Infinity and Infinity+ console, respectively. The experiments at 14.1 T were all performed at a spinning frequency of 25 kHz employing a double-resonance Varian APEX MAS probehead with a 2.5 mm stator. The experiments at 18.8 T were done at a spinning frequency of 50 kHz using a home-built double-resonance MAS probehead utilizing a Samoson 1.8 mm stator.[71] Zirconia rotors were used for all experiments. Processing of the NMR data was done using the matNMR[72] processing package.

4.3. Single-Pulse ^{17}O Spectrum. A single-pulse ^{17}O spectrum was obtained at an external field of 14.1 T and a spinning frequency of 25 kHz using a 2 μs excitation pulse with an ^{17}O rf field strength of 13.6 kHz. A total of 122880 transients were acquired with a recovery time interval of 0.35 s. TPPM decoupling[73] with a ^1H rf field strength of 96 kHz, pulse duration of 5.2 μs, and rf phases of ±30° was applied during signal acquisition. The ^{17}O signal of water was used as 0 ppm reference for the scale of the ^{17}O chemical shift. Prior to the ^{17}O single-pulse experiment, the spinning axis was set carefully to the magic angle with respect to the static magnetic field using a sample of $NaNO_3$.

The experimental ^{17}O spectrum was fitted to the ideal second-order quadrupolar powder line shape in the limit of very fast MAS.[74] Fitting parameters were the ^{17}O isotropic chemical shift δ_{iso}, the quadrupolar coupling constant C_Q, the asymmetry parameter η_Q, additional line broadening, and scaling factors for the intensity of the central and inner satellite transitions. The powder average was calculated using a set of 196418 pairs of $\{\alpha_{MR},\beta_{MR}\}$ angles chosen according to the ZCW scheme.[75]

4.3.1. Repetitive DFS. In all cases a PC-based arbitrary waveform generator from National Instruments (DAQArb PCI5411) was used to generate the amplitude modulation for the desired DFS on a carrier frequency of 14 MHz with a time resolution of 25 ns. This frequency is mixed into the spectrometer as described elsewhere.[20,76] The experiments performed at a static field of 14.1 T and a spinning frequency of 25 kHz employed a convergent DFS with starting and finishing resonance offsets of 2.5 MHz and 100 kHz, respectively. The ^{17}O rf field strength was 18 kHz and sweep duration was optimized to 4 ms in order to obtain maximum signal intensity. A total of 1968 transients were acquired with a recovery time interval of 10 s. For each transient a number of $n = 10$ DFS repetitions followed by signal detection was done. TPPM decoupling with a ^1H rf field strength of 109 kHz, pulse duration of 4.9 μs and rf phases of ±60° was applied during signal acquisition. For experiments at a static field of 18.8 T and spinning frequency of 50 kHz, a convergent DFS with starting and finishing frequencies of 2.5 MHz and 100 kHz, respectively, was used. The ^{17}O rf field strength and optimized sweep duration were set to 16 kHz and 6.8 ms, respectively. A total of 128 transients were acquired with a recovery time interval of 9 s. For each transient a number of $n = 10$ DFS repetitions followed by signal detection was done.

4.3.2. Heteronuclear Dipolar Recoupling. The recoupling experiments were performed at a static field of 18.8 T and a spinning frequency of 50 kHz. In all cases a divergent DFS was used with starting and finishing frequencies of 100 kHz and 1.4 MHz, respectively. The ^{17}O rf field strength and sweep duration were set to 17.5 kHz and 2 ms, respectively. Three different experiments were performed, each using a different heteronuclear recoupling sequence: (i) $(R12_3^5R12_3^{-5})3^1$. In this case no proton decoupling was used during the time interval $T - \tau$ and signal detection. The durations of the 90° and selective 180° pulses were given as 4.7 and 18 μs, respectively. (ii) $(R28_7^{13}R28_7^{-13})2^1$. (iii) $(R32_8^{15}R32_8^{-15})2^1$. In both cases (ii and iii) low power proton decoupling with a ^1H rf field strength of about 8−10 kHz was applied during the time interval $T - \tau$ and signal acquisition. The durations of the selective 90° and 180° pulses were given by 15 and 31 μs, respectively. In all three cases (i−iii) the ^1H rf field strength during the heteronuclear recoupling sequence was set to 100 kHz. To verify the exact setting of the rf field strength in each case, a complete proton two-dimensional (2D) nutation spectrum was acquired. The resulting rf profile allowed in addition to determine the rf inhomogeneity of the rf coil.

Numerically exact spin simulations were performed using SIMPSON.[77] In all cases powder averaging was accomplished using a set of 376 pairs of $\{\alpha_{MR},\beta_{MR}\}$ angles chosen according to the ZCW scheme[75] together with stepping the γ_{MR} angle equally from 0° to 360° in 19 steps; i.e., a total number of 7144 angle triplets was used. If not indicated otherwise, all spin interactions of the nuclei of interest were included in the simulations: (i) The experimental values of the $^{17}O^{\eta}$ quadrupolar coupling constant and asymmetry parameter, where the principal axis system as calculated by DFT was used. The first- and second-order quadrupolar coupling was included in the simulations, whereas the second-order cross term between the quadrupolar coupling and the heteronuclear $^{17}O-^1H$ dipolar coupling was ignored as discussed above. (ii) Heteronuclear $^{17}O-$

^{1}H and homonuclear ^{1}H−^{1}H dipolar couplings. (iii) Experimental offsets of the ^{17}O and ^{1}H spectrometer carrier frequencies. (iv) Chemical shielding tensors of the $^{17}O^{\eta}$, $^1H^{\eta}$, and $^1H''$ sites as determined by DFT calculations.

4.4. DFT Calculations. For the DFT calculations of the $^{17}O^{\eta}$ quadrupolar coupling, the $^{17}O^{\eta}$, $^1H^{\eta}$, and $^1H''$ chemical shift tensors in L-tyrosine·HCl the Amsterdam Density Functional (ADF) package[52−54] was used. Two clusters of L-tyrosine molecules were build from the neutron diffraction crystal structure:[78] The first one consisting of 10 L-tyrosine molecules together with 3 chlorine anions and 7 point charges at the positions of the other 7 chlorine anions. The second one consisting of 3 L-tyrosine molecules together with 1 chlorine anion and 2 point charges at the position of the other two chlorine anions.

In general, for all atoms in the molecular cluster a double-ζ polarized (DZP) atomic basis set was chosen. Exceptions were all the atoms in the central tyrosine molecule and the H″, O″, and C′ atoms of the tyrosine molecule, whose H″ is weakly hydrogen bonded to the O^{η} of the central tyrosine molecule, compare Figures 3 and 6. For those atoms a core double-ζ, valence triple-ζ, doubly polarized (T2ZP) basis set was chosen. In general, the basis set for N, C, and O atoms had a frozen 1s shell, while the basis set for the Cl atom had a frozen 2p shell. Exception is the O^{η} of the central tyrosine molecule, for which an all electron basis set was chosen.

In all cases we used two different pairs of exchange-and-correlation (XC) functionals: First, we employed the exchange and correlation corrections suggested in 1991 by Perdew and Wang, denoted PW91 (ref 79 and references therein). Second, we used the gradient correction proposed in 1988 by Becke[80] together with correlation correction introduced in 1988 by Lee, Yang, and Parr,[81] denoted BLYP. No relativistic effects were taken into account.

5. Results and Discussion

5.1. Single-Pulse ^{17}O Spectrum. Figure 3b shows the experimental single-pulse ^{17}O MAS spectrum of a powdered sample of $^{17}O^{\eta}$-L-tyrosine·HCl. The experimental spectrum was fitted to the ideal second-order quadrupolar line shape in the limit of fast MAS. The foot at about 100 ppm in the second-order central-transition line shape stems from the inner satellite transition in ^{17}O and was included in the fitting. As best fit values we obtained an isotropic chemical shift of $\delta_{iso} = 87.1 \pm 0.5$ ppm, a quadrupolar coupling constant of $C_Q = 8.52 \pm 0.05$ MHz, and an asymmetry parameter of $\eta_Q = 0.74 \pm 0.02$. Our results differ significantly from those presented earlier by Dupree and co-workers, who estimated values of $\delta_{iso} = 83 \pm 0.5$ ppm, $C_Q = 8.56 \pm 0.05$ MHz, and $\eta_Q = 0.65 \pm 0.02$.[9] Especially the difference in η_Q is evident, and we do not have any satisfying explanation for this deviation. One possibility could be slight differences in the $^{17}O^{\eta}$-L-tyrosine·HCl sample. We confirmed that indeed both the carboxyl and hydroxyl sites were protonated in our sample by recording ^{1}H spectra at 50 kHz spinning at an external field of 18.8 T (results not shown).

5.2. Repetitive DFS. Figure 4 shows the experimental results obtained using the rDFS pulse sequence in Figure 1 for $^{17}O^{\eta}$-L-tyrosine·HCl. The results in the first row (a) and (b) were obtained at an external field of $B_0 = 14.1$ T and a spinning frequency of $\omega_r/2\pi = 25$ kHz, while the results in the second row (c) and (d) were acquired at $B_0 = 18.8$ T using $\omega_r/2\pi = 50$ kHz. The individual FIDs, which were detected during the rDFS pulse sequence, are shown in the first column (a) and (c). The maximum signal enhancement is achieved by the first DFS. In the following repetitions, the signal enhancements decay approximately exponentially. The second column (b) and (d) shows the enhancement in the *S*/*N* ratio of the accumulated ^{17}O spectra using two different summation methods. First, the individual FIDs were summed directly without any weighting of the data. Since the *S*/*N* ratio in the individual FIDs drops with increasing number of repetitions, the *S*/*N* ratio of the summed signal also begins to drop again with increasing number of repetitions. This is circumvented by weighting each individual FID with its own intensity during summation. As a consequence, individual FIDs with a low *S*/*N* ratio get a small weighting factor. As a result the *S*/*N* ratio of the weighted sum of the individual FIDs continues to rise and levels off into a plateau with increasing number of repetitions. At a static field of 14.1 T and a spinning frequency of 25 kHz, we obtain enhancement factors for the ^{17}O signal of about 2.8 for a single DFS and 4.3 for 10 repetitive DFS. This result compares favorably with recent results obtained by Siegel et al. who reported a signal enhancement of 4.1 using a hyperbolic secant DFS for ^{27}Al under MAS condition in a powdered sample of aluminum acetylacetonate with a quadrupolar coupling constant of $C_Q = 3.03$ MHz and relatively small asymmetry parameter of $\eta_Q = 0.15$.[23]

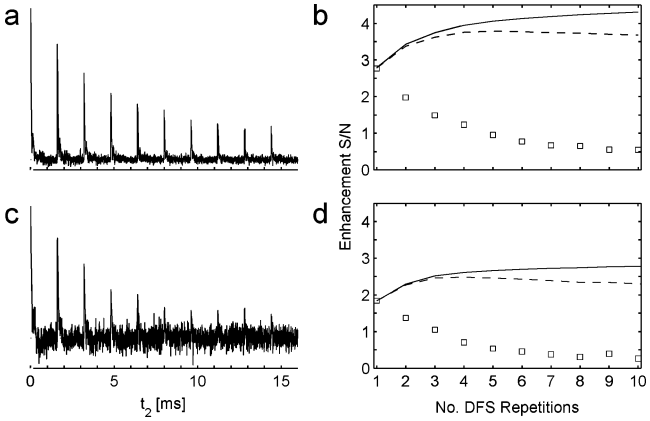

Figure 4. Experimental rDFS results on $^{17}O^{\eta}$-L-tyrosine·HCl. For (a) and (b) 1968 transients were recorded at a static field of 14.1 T and a spinning frequency of 25 kHz. For (c) and (d) 128 transients were recorded at a static field of 18.8 T and a spinning frequency of 50 kHz. (a) and (c) show the 10 individual ^{17}O FIDs acquired with the pulse sequence shown in Figure 1a. (b) and (d): Symbols: enhancement in the spectral *S*/*N* ratio for the individual FIDs during the rDFS sequence. Dashed lines: enhancement in the spectral *S*/*N* ratio if the sum of the individual FIDs is calculated. Solid lines: enhancement in the spectral *S*/*N* ratio for the weighted sum of the individual FIDs.

In the case of a static field of 18.8 T and a spinning frequency of 50 kHz, the enhancement is lower, a factor of 1.8 for a single DFS and 2.8 for 10 repetitive DFS is obtained. This is mainly attributed to the fact that the passages of the satellite transitions by each DFS on average gets less adiabatic the faster the sample is rotated.[76] Still these results show that DFS and rDFS are beneficial also in the regime of fast MAS. In general, we obtained the best results for sweeps using rf field strength of 10−20 kHz. In this regime the signal enhancement steadily increases as a function of the sweep duration until a plateau is reached.

The corresponding experimental ^{17}O spectra of $^{17}O^{\eta}$-L-tyrosine·HCl are shown in Figure 5. The first row (a−c) contains the results obtained at a static field of 14.1 T and a spinning frequency of 25 kHz, whereas the spectra in the second row (d−f) were acquired at a static field of 18.8 T and a spinning frequency of 50 kHz. The left-hand column (a and d) shows the reference spectra obtained with a selective 90° pulse on the

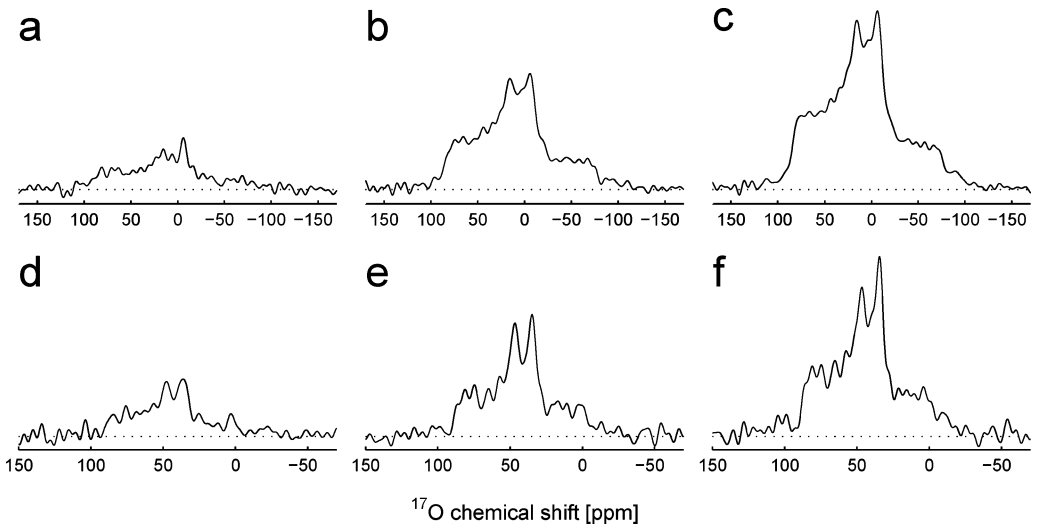

Figure 5. Experimental ^{17}O spectra of $^{17}O^{\eta}$-L-tyrosine·HCl. (a−c) 1968 transients, external field of 14.1 T, and 25 kHz spinning frequency. (d−f) 128 transients, external field of 18.8 T, and 50 kHz spinning frequency. (a and d) Spectra obtained with a selective 90° pulse on the central transition equilibrium magnetization. (b and e) Spectra obtained after a applying a single DFS prior to the 90° selective pulse. (c and f) Spectra obtained by a weighted sum of the individual FIDs acquired during the rDFS sequence.

TABLE 1: (a) Experimental Result for the $^{17}O^{\eta}$ Isotropic Chemical Shift and the Quadrupolar Coupling Constant and Asymmetry Parameter, (b) Results of DFT Calculations for the $^{17}O^{\eta}$ Quadrupolar Coupling Tensor, and (c) Results of DFT Calculations for Different Chemical Shift Tensors[a]

(a) Experimental Results

nucleus	δ_{iso} (ppm)	χ_Q (MHz)	η_Q	SIMPSON
$^{17}O^{\eta}$	87.1 ± 0.5	8.52 ± 0.05	0.74 ± 0.02	*

(b) DFT Calculations: Quadrupole Coupling

nucleus	XC	cluster	χ_Q (MHz)	η_Q	Ω^Q_{PM} (deg)	SIMPSON
$^{17}O^{\eta}$	PW91	3	8.61	0.74	{−99, 49, 89}	
$^{17}O^{\eta}$	BLYP	3	8.69	0.74	{−99, 49, 89}	
$^{17}O^{\eta}$	PW91	10	8.66	0.82	{−99, 45, 89}	*
$^{17}O^{\eta}$	BLYP	10	8.75	0.82	{−99, 45, 89}	

(c) DFT Calculations: CSA

nucleus	XC	cluster	δ_{aniso} (ppm)	η	Ω^{CSA}_{PM} (deg)	SIMPSON
$^{17}O^{\eta}$	PW91	3	47.6	0.75	{− 96, 27, −81}	
$^{17}O^{\eta}$	BLYP	3	46.5	0.70	{−96, 28, −80}	*
$^{17}O^{\eta}$	PW91	10	39.0	0.65	{−101, 30, −81}	
$^{17}O^{\eta}$	BLYP	10	38.0	0.60	{−102, 31, −80}	
$^{1}H^{\eta}$	PW91	3	−23.9	0.43	{−72, 168, −77}	
$^{1}H^{\eta}$	BLYP	3	−23.9	0.43	{−72, 169, −77}	*
$^{1}H^{\eta}$	PW91	10	−21.1	0.32	{−81, 170, −81}	
$^{1}H^{\eta}$	BLYP	10	−21.1	0.32	{−80, 170, −81}	
$^{1}H''$	PW91	3	−18.6	0.36	{71, 119, 55}	
$^{1}H''$	BLYP	3	−18.6	0.35	{71, 120, 55}	*
$^{1}H''$	PW91	10	−17.5	0.10	{85, 119, 52}	
$^{1}H''$	BLYP	10	−17.5	0.10	{85, 119, 52}	

[a] The anisotropic deshielding constant δ_{aniso} and the asymmetry parameter η of the chemical shift tensor are defined in section 3.2 below eq 13. In the case of (b) and (c) the Euler angles Ω^{Λ}_{PM} give the relative orientation of the interaction tensor Λ and a molecule fixed frame with its *z*-axis along the $O^{\eta}-H^{\eta}$ internuclear vector and its *x*-axis perpendicular to the $C^{\zeta}-O^{\eta}-H^{\eta}$ plane (compare Figure 6). The columns marked "XC" and "Cluster" indicate the exchange-and-correlation functionals and sizes of the molecular clusters used in the calculations, respectively. An asterisk in the column "SIMPSON" indicates those results which have been used in the numerical heteronuclear recoupling spin simulations.

central transition starting at thermal equilibrium. The results in the center column (b and e) stem from the application of a single DFS prior to the selective 90° pulse. The right column (c and f) contains the results using the rDFS sequence and forming the weighted sum of 10 individual FIDs. It should be noted that the noise levels are identical for all spectra in the same row. The enhancement in the *S*/*N* ratio plotted in Figure 4 can therefore be observed by comparing the spectral intensities. In addition it becomes clear that both applying a single DFS or the rDFS preserves the second-order quadrupolar line shape.

5.3. DFT Calculations. We performed DFT calculations of the ^{17}O quadrupolar coupling tensor in $^{17}O^{\eta}$-L-tyrosine·HCl. In addition we calculated the chemical shift tensor of the $^{17}O^{\eta}$, $^{1}H^{\eta}$, and $^{1}H''$ sites. The results are collected in Table 1. Figure 6 shows the principal axis system of the $^{17}O^{\eta}$ quadrupolar tensor and the $^{1}H^{\eta}$ chemical shift tensor

The value of the quadrupolar coupling constant C_Q lies in the range 8.61−8.75 MHz for all calculations, showing that this parameter is only limitedly affected by the choice of cluster size. The choice of the XC functional has a larger influence on

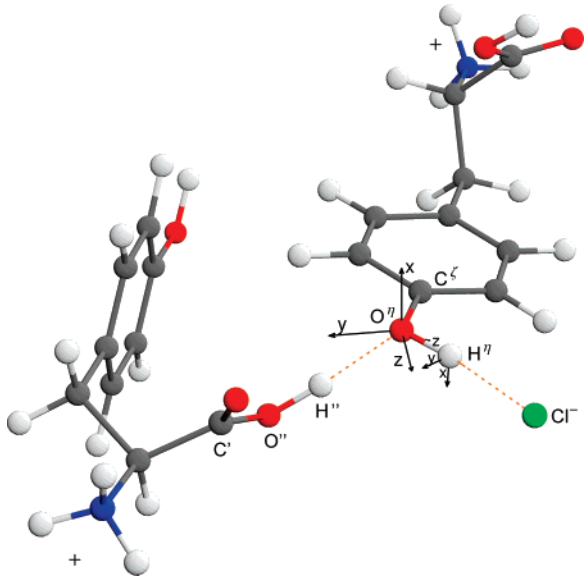

Figure 6. Two adjacent L-tyrosine cations and one chlorine anion in the neutron diffraction crystal structure[78] of L-tyrosine·HCl. The principal axis systems of the $^{17}O^{\eta}$ quadrupole coupling tensor and of the $^{1}H^{\eta}$ chemical shift tensor obtained by DFT calculations (results marked with asterisks in Table 1) are indicated.

the final result. For the asymmetry parameter η_Q the situation is reversed: For each cluster size the values are about the same for the different XC functionals, but they are significantly different for different cluster sizes. It should be noted that the deviation of the calculated values from the experimental results is larger for the 10 molecule cluster than for the 3 molecule cluster. Gervais et al. calculated values of $C_Q = 8.60$ MHz and $\eta_Q = 0.8$ taking the periodicity of the crystal into account explicitly.[51] Our results for the 10 molecular cluster are quite close to these values.

There is still a notable discrepancy between the calculated and measured values for η_Q for the $^{17}O^{\eta}$ site in L-tyrosine·HCl, both for the cluster and periodic calculations. For carboxylic ^{17}O sites the observed differences are usually much smaller, as has been shown for various amino acids.[51] We do not fully understand this discrepancy for the hydroxyl $^{17}O^{\eta}$ site at this point. However, the asymmetry parameter of carbonyl oxygens is apparently determined more locally with its high electron density in the double bond, whereas the asymmetry parameter of hydroxyl oxygens is stronger influenced by long-range variations in the electron density. It seems generally true that the size of the quadrupolar interaction is determined more locally, whereas the site symmetry contains some longer range effects. We conclude that the quadrupolar coupling constant may be calculated quite well using small molecular clusters, while the asymmetry parameter generally requires a larger cluster size. The orientation of the principal axis system of the quadrupolar tensor is essentially identical for all the different calculations and is shown in Figure 6. The *x*-axis is almost perpendicular to the $C^{\zeta}-O^{\eta}-H^{\eta}$ plane. The *z*-axis is rotated away from the $O^{\eta}-H^{\eta}$ bond around the *x*-axis by about 45°−49° in the negative sense.

In case of the $^{17}O^{\eta}$ chemical shift tensor the differences for both the value of the anisotropic deshielding δ_{aniso} and the asymmetry parameter η are significantly different for the different cluster sizes, whereas the choice of another XC functional has less of an influence on the calculated results. The results of Gervais et al. obtained by periodic calculations correspond to $\delta_{aniso} = 40.9$ ppm and $\eta = 0.75$ for the $^{17}O^{\eta}$ CSA.[51] The value of δ_{aniso} is very close to our results for the 10 molecule cluster, while the value of η shows a discrepancy that is larger for the 10 molecule cluster than for the 3 molecule cluster. This discrepancy seems to stem from the chosen XC functional. Furthermore, the Euler angles describing the relative orientation of the chemical shift and quadrupolar tensor reported by Gervais et al. are very close to our results, which can be deduced from Table 1 (values not shown). In the case of the $^{1}H^{\eta}$ and $^{1}H''$ chemical shift tensors, the values for η depend strongly on the choice of the cluster size. The *z*-axis of the principal axis systems of the proton chemical shift tensors is in all cases almost collinear with the O−H bonds as expected.

Pike et al. have experimentally determined the ^{17}O quadrupolar coupling constants and asymmetry parameters in different amino acids.[9] However no distinct correlation between the size of quadrupolar coupling constant and the length of N−H···O and O−H···O hydrogen bonds could be observed, whereas the principal components of the ^{17}O chemical shift tensor depend linearly on the hydrogen bonding distance.[51] We performed a series of DFT calculations in L-tyrosine·HCl using a 10 molecule cluster varying the $O^{\eta}-H^{\eta}$ bond length of the central tyrosine molecule in the range from 99 to 105 pm. This serves as a simple model for the effect of O−H···O hydrogen bonding to elongate the O−H bond length. The resulting calculated values for the O^{η} quadrupolar coupling constant decrease linearly from 8.66 to 8.57 MHz. This corresponds to a change in the quadrupolar coupling constant of about −0.016 MHz per 1 pm increase in the $O^{\eta}-H^{\eta}$ bond length. This value is rather small, and therefore a very accurate determination of the quadrupolar coupling constant would be required to deduce the $O^{\eta}-H^{\eta}$ bond length from the quadrupolar coupling constant. Therefore a more direct and accurate method to characterize hydrogen bonding is measuring internuclear $^{17}O-^{1}H$ distances as was discussed in theory in section 3. Numerical simulations and experimental results of these experiments will be shown in the following section.

5.4. Heteronuclear $^{17}O-^{1}H$ Dipolar Recoupling. 5.4.1. Numerical Simulations. We performed numerically exact spin simulations of the different heteronuclear longitudinal two-spin-order recoupling sequences in eq 4 and supercycles in eq 5 together with the basic element $\mathcal{R} = 180_0$ to assess their robustness in the presence of ^{17}O quadrupolar coupling and ^{17}O and ^{1}H chemical shift anisotropy. We found in general that the sequences $(R32_8^{15}R32_8^{-15})2^1$ and $(R32_8^{15}R32_8^{-15})3^1$ showed the best performance. Figure 7 shows the simulated ^{17}O spin-echo signal amplitudes as a function of the duration τ of the recoupling sequence. Parts a and b of Figure 7 are calculated for two different heteronuclear dipolar couplings, 14500 and 3909 Hz, respectively, comparing the results for these two sequences using either numerical two-spin simulations considering in each case all relevant spin interactions as described in section 4.3.2 or the average Hamiltonian results as given in eq 15, i.e., considering solely the actual heteronuclear dipolar coupling of interest. In each case the curves of all calculations are almost identical demonstrating the robustness of both recoupling sequences with respect to ^{17}O quadrupolar couplings and both ^{17}O and ^{1}H chemical shift anisotropies.

We found that the influence of the ^{17}O quadrupolar coupling and chemical shift anisotropy on the numerically simulated dephasing curves is negligible. Therefore the ^{1}H chemical shift anisotropy is responsible for the slight deviations of the results obtained by numerical simulations and by average Hamiltonian calculations. It should be noted that the size the anisotropic chemical shift of hydroxyl and carboxylic protons is quite large,

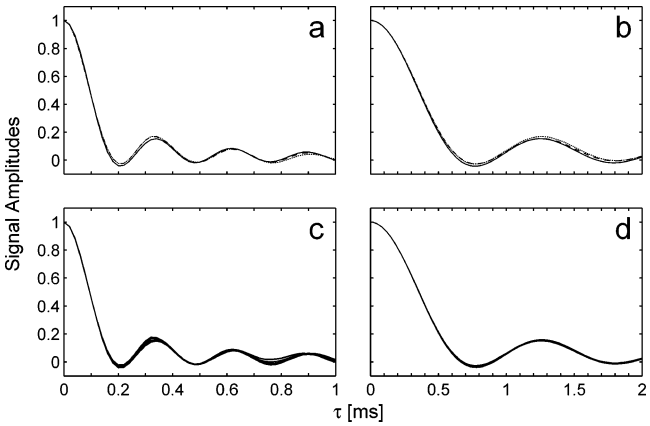

Figure 7. Simulated ^{17}O spin-echo signal amplitudes in the presence of different heteronuclear recoupling pulse sequences of duration τ in $^{17}O^{\eta}$-L-tyrosine·HCl for an external field of 18.1 T and spinning frequency of 50 kHz. (a and c) A two spin system consisting of $^{17}O^{\eta}$ and $^{1}H^{\eta}$. A heteronuclear dipolar coupling constant of $b_{IS}/2\pi = 14500$ Hz was used. (b and d) A two spin system consisting of $^{17}O^{\eta}$ and $^{1}H''$. The heteronuclear dipolar coupling constant was $b_{IS}/2\pi = 3909$ Hz. (a and b) Dotted lines: numerically exact simulations for the sequence $(R32_8^{15}R32_8^{-15})2^1$ considering all relevant spin interactions. Dashed lines: numerical simulations for the sequence $(R32_8^{15}R32_8^{-15})3^1$ considering all relevant spin interactions. Solid lines: average Hamiltonian simulations according to eq 15, only considering the heteronuclear dipolar couplings. (c) numerical simulations for the sequence $(R32_8^{15}R32_8^{-15})3^1$ as in (a) but assuming an ensemble of 50 random orientations of the $^{1}H^{\eta}$ chemical shift tensor. (c) numerically exact simulations for the sequence $(R32_8^{15}R32_8^{-15})3^1$ as in (b) but assuming and ensemble of 50 random orientations of the $^{1}H''$ chemical shift tensor. For all numerically exact simulations the selective 180° pulse on the ^{17}O central transition in the center of the spin-echo sequence was assumed to be ideal.

i.e., on the order of 21−24 ppm (16.8−19.2 kHz at a static field of 18.8 T) for the $^{1}H^{\eta}$ site. As the recoupled proton CSA commutes with the heteronuclear ^{17}O−^{1}H dipolar interaction in the first-order average Hamiltonian for the sequences employed here, its influence is minor as underpinned by parts a and b of Figure 7. Parts c and d of Figure 7 support this, since the dependence on the orientation of the ^{1}H chemical shift tensor is also quite small.

5.4.2. Experimental Results. Experimental modulation curves for different heteronuclear recoupling sequences obtained using the pulse sequence in Figure 1 for $^{17}O^{\eta}$-L-tyrosine·HCl at a static field of 18.8 T and a spinning frequency of 50 kHz are shown in Figure 8. The normalized experimental integrals of the $^{17}O^{\eta}$ spectral peak (complete second-order line shape) are plotted as a function of the duration τ of the recoupling pulse sequence. The peak integrals were in all cases normalized to the peak integral at $\tau = 0$. The results in Figure 8 were obtained using the following recoupling sequences: (a) $(R12_3^5R12_3^{-5})3^1$, (b) $(R28_7^{13}R28_7^{-13})2^1$ and (c) $(R32_8^{15}R32_8^{-15})2^1$.

The solid lines in Figure 8 are a result of numerically exact spin simulations using all relevant spin interactions. The numerical simulations were multiplied by an exponential damping factor $f \exp\{-\tau/T_R\}$ to take relaxation into account. In addition we had to add an empirical exponentially damped constant offset $(1 - f) \exp\{-\tau/T_{qe}\}$ to satisfactorily fit the calculated curves to the experimental signal intensities. We attribute this offset to the complex relaxation pathways in the proton network that leads to a decaying quasi-equilibrium state.[82] A similar offset has been used to describe the two-spin dynamics at the rotational resonance condition in a multiple spin system.[83] This approach requires that actual heteronuclear dipolar *oscillations* are observed in order to obtain the heteronuclear dipolar coupling by fitting the experimental results to simulations. A plain *dephasing* (or damping) of the signal by the heteronuclear dipolar coupling would be obscured by relaxation and only a qualitative estimate of the heteronuclear dipolar coupling would be possible. Apart from the heteronuclear dipolar coupling we therefore considered three further fitting parameters: the exponential damping and the exponentially damped offset. We obtained the 95% confidence interval for the heteronuclear dipolar coupling by calculating the mean squared deviation S between the experimental and simulated amplitudes for a series of different heteronuclear dipolar couplings, where the other three fitting parameters were optimized as to minimize S in each case. The 95% confidence interval is determined by the set of dipolar couplings for which $S \leq S_{min}\{1 + F_{1,n-4}^{0.05}/(n - 4)\}$, where S_{min} is the mean squared deviation between experimental and simulated amplitudes minimized by optimizing all four fitting parameters and n is the number of experimental points.

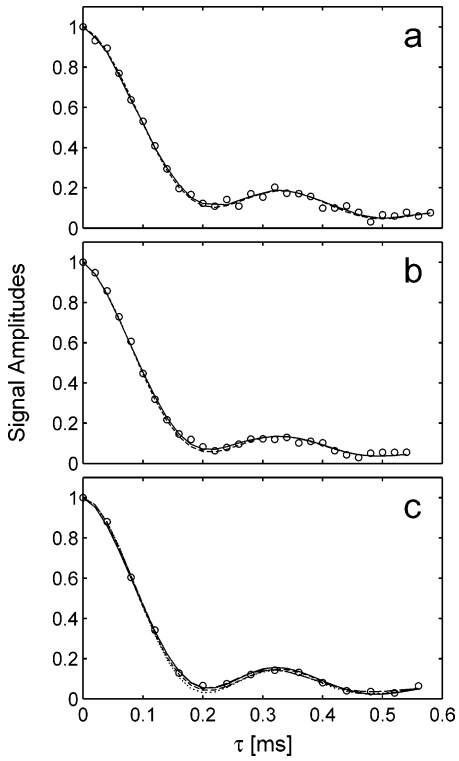

Figure 8. Symbols: Normalized experimental integrals of the $^{17}O^{\eta}$ spectral peak for different heteronuclear recoupling pulse sequences as a function of the recoupling interval τ. The data were acquired for $^{17}O^{\eta}$-L-tyrosine·HCl in an external field of 18.1 T and at a spinning frequency of 50 kHz. The following recoupling sequences were used: (a) $(R12_3^5R12_3^{-5})3^1$, (b) $(R28_7^{13}R28_7^{-13})2^1$, (c) $(R32_8^{15}R32_8^{-15})2^1$. Solid lines: best fit two-spin numerical simulations of the amplitudes multiplied by an exponential function and added to an exponentially damped constant offset. The following results were obtained for the heteronuclear dipolar $^{17}O^{\eta}-^{1}H^{\eta}$ coupling constants, the factor f and the relaxation time constants T_R and T_{qe}: (a) $(b_{IS}/2\pi, f, T_R, T_{qe}) = (14270 \pm 380$ Hz, 0.75, 1.61 ms, 0.34 ms), (b) $(b_{IS}/2\pi, f, T_R, T_{qe}) = (14410 \pm 370$ Hz, 0.87, 0.57 ms, 0.43 ms), (c) $(b_{IS}/2\pi, f, T_R, T_{qe}) = (14610 \pm 370$ Hz, 0.87, 1.02 ms, 0.35 ms). Short-dashed lines: Average Hamiltonian two-spin simulations according to eq 15 using the same parameters as for the solid lines. Long-dashed line in (c): best fit numerical simulations for a $^{17}O^{\eta}-^{1}H^{\eta}$ dipolar coupling constant of 14560 ± 290 Hz assuming a three spin system of $^{17}O^{\eta}$, $^{1}H^{\eta}$, and $^{1}H''$. The factor f and the relaxation time constants T_R and T_{qe} are given by $(f, T_R, T_{qe}) = (0.90, 2.88$ ms, 0.76 ms). Dotted line in (c): Average Hamiltonian three-spin simulation using the same parameters as for the long-dashed line.

$F^{\alpha}(p_1, p_2)$ is the upper α probability point of the F distribution with p_1 and p_2 degrees of freedom.[84]

In case of Figures 8a−c a two spin system consisting of $^{17}O^{\eta}$ and $^{1}H^{\eta}$ was assumed for the simulations. In case of Figure 8c in addition an alternative fit with a three-spin system composed of $^{17}O^{\eta}$, $^{1}H^{\eta}$, and $^{1}H''$ was used, where the $^{17}O^{\eta}-^{1}H''$ dipolar coupling was set to 3909 Hz (distance 160.9 pm) from the neutron diffraction crystal structure, the $^{17}O^{\eta}-^{1}H^{\eta}$ was varied during the fitting procedure and the homonuclear $^{1}H^{\eta}-^{1}H''$ coupling each time adjusted accordingly. The best fits for the heteronuclear dipolar coupling constants assuming a two-spin system of $^{17}O^{\eta}$ and $^{1}H^{\eta}$ are given by (a) 14270 ± 380 Hz, (b) 14410 ± 370 Hz, and (c) 14610 ± 370 Hz. The best fit value for the $^{17}O^{\eta}-^{1}H^{\eta}$ heteronuclear dipolar coupling constant using a three-spin system is given by 14560 ± 290 Hz. The spread in the results is quite small, and all values lie within the confidence intervals of each measurement. The experimental results in Figure 8c were obtained using the $(R32_8^{15}R32_8^{-15})2^1$ sequence and show the smoothest and deepest oscillations. Since this sequence furthermore showed also the best robustness with respect to the ^{1}H CSA, we consider these results slightly more reliable. It should be noted that the results considering a two- or three-spin system in the numerical simulations, respectively, differ just by 50 Hz, which is very small compared to the confidence interval in the order of ±290−370 Hz. A $^{17}O^{\eta}-^{1}H^{\eta}$ dipolar coupling constant of 14560 ± 290 Hz corresponds to an internuclear distance of $r_{NMR} = 103.8 \pm 0.7$ pm. This is about 5% larger than the distance of $r_{n-diff} = 98.9$ pm estimated by neutron diffraction, which corresponds to a heteronuclear dipolar coupling constant of 16840 Hz. Therefore the observed dipolar coupling constant is about 13.5% smaller than the one calculated from the neutron structure. Although these discrepancies are significant, they can be explained by the librational motion of the $^{17}O^{\eta}-^{1}H^{\eta}$ bond vector: Ishii et al. calculated by molecular dynamics simulations in glycine that C−H and N−H distances measured by NMR at 273 K are 3.7−5.3% longer than the distances estimated by neutron diffraction.[85] Even at 0 K the zero-point librational motion still results in discrepancies in the order of 2−3%.[85,86] The value of r_{NMR} at 0 K can be determined by extrapolating the results of NMR measurements performed at different temperatures.[85] In general the discrepancies are much larger for direct bonds involving hydrogen atoms than for direct bonds not involving hydrogen atoms. Van Beek et al. observed discrepancies in their solid-state NMR estimation of $^{17}O-^{1}H$ distances in $Mg(^{17}OH)_2$ and [U-^{13}C,^{17}O]-glycine·HCl between r_{NMR} and r_{n-diff} of 12.6% and 8.9%, respectively.[50] Considering the fact they studied different samples and used a different recoupling sequence, no unambiguous statements as why they find larger bond length differences are possible.

The short-dashed and dotted lines in Figure 6 are the result of average Hamiltonian calculation according to eq 15 using the same parameters as for the numerical exact simulations. In general the agreement with the numerically exact simulations is very good. Just in the case of the three spin simulations in Figure 8d, a small difference can be observed. Therefore the analysis of the experimental curves may for simplicity be done just using average Hamiltonian calculations, which are much less elaborate than numerically exact simulations.

6. Conclusions

In this paper we showed that double frequency sweeps are a robust and easy to optimize technique to enhance the *S*/*N* ratio in ^{17}O solid-state NMR of biological samples. We could further improve the enhancement in sensitivity by the repetitive DFS pulse sequence. As a result a maximum enhancement in the *S*/*N* ratio by a factor of 4.3 in $^{17}O^{\eta}$-L-tyrosine·HCl was experimentally demonstrated at an external field of 14.1 T and a spinning frequency of 25 kHz. Furthermore, as little as 128 transients lead to meaningful ^{17}O spectra of the same sample at an external field of 18.8 T and a spinning frequency of 50 kHz. Therefore DFS and rDFS are compatible with high magnetic fields and fast magic-angle sample spinning, paving the way for more complex experiments under these conditions. Furthermore, both techniques preserve the quadrupolar powder line shape. As a result DFS, rDFS, and experiments based on them are expected to be of great importance in the ^{17}O solid-state NMR of more complex biological and biomimetic systems. This allows accurate determination of C_Q and η_Q needed to interpret small but significant changes in these parameters as a result of differences in hydrogen bonding. However, since these changes are small, a more direct and accurate way to characterize hydrogen bonding is to determine $^{17}O-^{1}H$ distances. Such distance measurements and more in general multidimensional experiments benefit crucially from the enhancement in the *S*/*N* ratio obtained by employing DFS and rDFS schemes.

In addition, we performed DFT calculations of the $^{17}O^{\eta}$ quadrupolar coupling tensor and the $^{17}O^{\eta}$, $^{1}H^{\eta}$ and $^{1}H''$ chemical shift tensors in L-tyrosine·HCl. We observed that in the case of the ^{17}O quadrupolar coupling tensor, only the asymmetry parameter depends on the size of the molecular cluster chosen for the calculations. In the case of the ^{17}O and ^{1}H chemical shift tensors, both the anisotropic shift and the asymmetry parameter are sensitive to the cluster size. A comparison of our ^{17}O results for a 10 molecule cluster with the findings of Gervais et al., who took the periodicity of the crystal into account explicitly,[51] shows good agreement. DFT calculations are an important tool to support the interpretation of ^{17}O solid-state NMR results in biological and biomimetic systems.

We employed supercycled symmetry-based RN_n^{ν} pulse sequences on the proton channel to achieve heteronuclear longitudinal two-spin-order recoupling to determine $^{17}O-^{1}H$ distances. These sequences recouple the heteronuclear dipolar $^{17}O-^{1}H$ couplings while decoupling the homonuclear proton dipolar interactions. Since the recoupled heteronuclear dipolar interactions commute for different spin pairs, these sequences do not suffer from dipolar truncation. The proton CSA terms, which are simultaneously recoupled in first-order average Hamiltonian, commute with the heteronuclear dipolar coupling terms. That allows the design of experiments where the measurement of $^{17}O-^{1}H$ heteronuclear dipolar couplings is hardly influenced by the ^{1}H chemical shift interactions. We further stabilized the performance of the sequences by implementing a combination of inversion and MQ supercycles. It should be noted that the symmetry-allowed second-order cross terms between the ^{17}O quadrupolar coupling and the $^{17}O-^{1}H$ heteronuclear dipolar coupling are small at the high external fields chosen here and therefore need not be considered. Two of the most promising heteronuclear longitudinal two-spin-order recoupling sequences are $(R32_8^{15}R32_8^{-15})2^1$ and $(R32_8^{15}R32_8^{-15})3^1$, where the choice of the MQ phase cycle is determined by the size of the targeted heteronuclear coupling, i.e., the maximal duration of the heteronuclear recoupling. We demonstrated the sequence $(R32_8^{15}R32_8^{-15})2^1$ experimentally by estimating the $^{17}O^{\eta}-^{1}H^{\eta}$ distance in $^{17}O^{\eta}$-L-tyrosine·HCl at a spinning frequency of 50 kHz in an external magnetic field of 18.8 T. Our result for the $^{17}O^{\eta}-^{1}H^{\eta}$ NMR distance of 103.8 ± 0.7 pm is about 5% larger than the value of 98.9 pm estimated by neutron diffraction,

which may be explained by the librational motion of the $^{17}O^{\eta}-{}^{1}H^{\eta}$ bond vector. The symmetry-based heteronuclear longitudinal two-spin-order recoupling sequences may be readily used in experiments to measure certain internuclear $^{17}O-{}^{1}H$ distances selectively following the approach established for the widely used REDOR sequence,[87,88] and progress in this direction combined with further improvements in the symmetric sequence design is under way in our laboratory. In addition, the sequences can be incorporated into existing experiments which use rotor-encoding of spin-pair coherences in a second time dimension to determine internuclear distances.[45] It is also possible to use them in the single- or multiple-quantum dimension in MQMAS experiments, following the approach in refs 43 and 44. All these experiments will benefit from the better homonuclear decoupling properties of the symmetry-based recoupling sequences. Furthermore, these experiments can be used for magnetization transfer from protons to ^{17}O, thus allowing two-dimensional NMR spectra to be obtained which correlate the chemical shifts of ^{1}H and ^{17}O sites close in space. Finally it should be mentioned that the application of the symmetry-based heteronuclear longitudinal two-spin-order recoupling sequences is not limited to the determination of internuclear $^{17}O-{}^{1}H$ distances only. As they are applied to the protons, they will be advantageous over existing techniques to determine distances between protons and heteronuclei in general, irrespective of their spin quantum number.

Acknowledgment. We thank Jan van Os, Gerrit Janssen, and Hans Janssen for experimental help, Erik van Lenthe for the ADF support, Ernst van Eck, Niels Nielsen, Jacco van Beek, and Malcolm Levitt for discussions, and the latter two in addition for a preprint of ref 50. A.B. has been supported by the VENI Grant 700.52.409 by The Netherlands Organization for Scientific Research (NWO).

References and Notes

(1) Jeffrey, G. A. *An Introduction to Hydrogen Bonding;* Oxford University Press: New York, 1997.
(2) Steiner, T. *Angew. Chem., Int. Ed.* **2002**, *41*, 48−76.
(3) Wu, G.; Dong, S. *J. Am. Chem. Soc.* **2001**, *123*, 9119−9125.
(4) Wu, G.; Dong, S. *Chem. Phys. Lett.* **2001**, *334*, 265−270.
(5) Zhang, Q.; Chekmenev, E. Y.; Wittebort, R. J. *J. Am. Chem. Soc.* **2003**, *125*, 9140−9146.
(6) Lemaître, V.; Smith, M. E.; Watts, A. *Solid State NMR* **2004**, *26*, 215−235.
(7) Wu, G.; Dong, S.; Ida, R.; Reen, N. *J. Am. Chem. Soc.* **2002**, *124*, 1768−1777.
(8) Lemaître, V.; Pike, K. J.; Watts, A.; Anupold, T.; Samoson, A.; Smith, M. E.; Dupree, R. *Chem. Phys. Lett.* **2003**, *371*, 91−97.
(9) Pike, K. J.; Lemaitre, V.; Kukol, A.; Anupõld, T.; Samoson, A.; Howes, A. P.; Watts, A.; Smith, M. E.; Dupree, R. *J. Phys. Chem. B* **2004**, *108*, 9256−9263.
(10) Prasad, S.; Clark, T. M.; Sharma, R.; Kwak, H.-T.; Grandinetti, P. J.; Zimmermann, H. *Solid State NMR* **2006**, *29*, 119−124.
(11) Yamauchi, K.; Kuroki, S.; Ando, I.; Ozaki, T.; Shoji, A. *Chem. Phys. Lett.* **1999**, *302*, 331−336.
(12) Yamauchi, K.; Kuroki, S.; Ando, I. *J. Mol. Struct.* **2002**, *602*−*603*, 171−175.
(13) Lemaître, V.; de Planque, M. R. R.; Howes, A. P.; Smith, M. E.; Dupree, R.; Watts, A. *J. Am. Chem. Soc.* **2004**, *126*, 15320−15321.
(14) Hu, J.; Chekmenev, E. Y.; Gan, Z.; Gor'kov, P. L.; Saha, S.; Brey, W. W.; Cross, T. A. *J. Am. Chem. Soc.* **2005**, *127*, 11922−11923.
(15) Vega, S.; Naor, Y. *J. Chem. Phys.* **1981**, *75*, 75−86.
(16) Haase, J.; Conradi, M. S. *Chem. Phys. Lett.* **1993**, *209*, 287−291.
(17) Kentgens, A. P. M.; Verhagen, R. *Chem. Phys. Lett.* **1999**, *300*, 435−443.
(18) Madhu, P. K.; Goldbourt, A.; Frydman, L.; Vega, S. *J. Chem. Phys.* **2000**, *112*, 2377−2391.
(19) Yao, Z.; Kwak, H.-T.; Sakellariou, D.; Emsley, L.; Grandinetti, P. J. *Chem. Phys. Lett.* **2000**, *327*, 85−90.
(20) Schäfer, H.; Iuga, D.; Verhagen, R.; Kentgens, A. P. M. *J. Chem. Phys.* **2001**, *114*, 3073−3091.
(21) Iuga, D.; Kentgens, A. P. M. *J. Magn. Reson.* **2002**, *158*, 65−72.
(22) Siegel, R.; Nakashima, T. T.; Wasylishen, R. E. *Chem. Phys. Lett.* **2004**, *388*, 441−445.
(23) Siegel, R.; Nakashima, T. T.; Wasylishen, R. E. *Chem. Phys. Lett.* **2006**, *421*, 529−533.
(24) Kwak, H.-T.; Prasad, S.; Clark, T.; Grandinetti, P. J. *Solid State NMR* **2003**, *24*, 71−77.
(25) Kentgens, A. P. M.; van Eck, E. R. H.; Ajithkumar, T.; Anupõld, T.; Past, J.; Reinhold, A.; Samoson, A. *J. Magn. Reson.* **2006**, *178*, 212−219.
(26) van Eck, E. R. H.; Smith, M. E. *J. Chem. Phys.* **1998**, *108*, 5904−5912.
(27) Goldburg, W. I.; Lee, M. *Phys. Rev. Lett.* **1963**, *11*, 255−258.
(28) Bennett, A. E.; Griffin, R. G.; Vega, S. *NMR: Basic Princ Prog.* **1994**, *33*, 1−77.
(29) Dusold, S.; Sebald, A. *Annu. Rep. NMR Spectrosc.* **2000**, *41*, 185−264.
(30) Levitt, M. H. Symmetry-Based Pulse Sequences in Magic-Angle Spinning Solid-State NMR. In *Encyclopedia of Nuclear Magnetic Resonance*; Grant, D. M., Harris, R. K., Eds.; Wiley: Chichester, England, 2002; Vol. 9.
(31) Brinkmann, A.; Levitt, M. H. *J. Chem. Phys.* **2001**, *115*, 357−384.
(32) Pines, A.; Gibby, M. G.; Waugh, J. S. *J. Chem. Phys.* **1973**, *59*, 569−590.
(33) Vega, A. J. *J. Magn. Reson.* **1992**, *96*, 50−68.
(34) Mali, G.; Kaučič, V. *J. Chem. Phys.* **2002**, *117*, 3327−3339.
(35) Gullion, T.; Schaefer, J. *J. Magn. Reson.* **1989**, *81*, 196−200.
(36) Gullion, T.; Vega, A. J. *Prog. NMR Spectrosc.* **2005**, *47*, 123−136.
(37) Hing, A. W.; Vega, S.; Schaefer, J. *J. Magn. Reson.* **1992**, *96*, 205−209.
(38) Gullion, T. *Chem. Phys. Lett.* **1995**, *246*, 325−330.
(39) Goldbourt, A.; Vega, S.; Gullion, T.; Vega, A. J. *J. Am. Chem. Soc.* **2003**, *125*, 11194−11195.
(40) van Eck, E. R. H.; Janssen, R.; Maas, W. E. J. R.; Veeman, W. S. *Chem. Phys. Lett.* **1990**, *174*, 428−432.
(41) Baldus, M.; Meier, B. H. *J. Magn. Reson.* **1997**, *128*, 172−193.
(42) Frydman, L.; Harwood: J. S. *J. Am. Chem. Soc.* **1995**, *117*, 5367−5368.
(43) Fernandez, C.; Lang, D. P.; Amoureux, J. P.; Pruski, M. *J. Am. Chem. Soc.* **1998**, *120*, 2672−2673.
(44) Pruski, M.; Bailly, A.; Lang, D. P.; Amoureux, J. P.; Fernandez, C. *Chem. Phys. Lett.* **1999**, *307*, 35−40.
(45) Saalwächter, K.; Graf, R.; Spiess, H. W. *J. Magn. Reson.* **2001**, *148*, 398−418.
(46) Lupulescu, A.; Brown, S. P.; Spiess, H. W. *J. Magn. Reson.* **2002**, *154*, 101−129.
(47) Carravetta, M.; Edén, M.; Zhao, X.; Brinkmann, A.; Levitt, M. H. *Chem. Phys. Lett.* **2000**, *321*, 205−215.
(48) Zhao, X.; Edén, M.; Levitt, M. H. *Chem. Phys. Lett.* **2001**, *342*, 353−361.
(49) Zhao, X.; Sudmeier, J. E.; Bachovchin, W. W.; Levitt, M. H. *J. Am. Chem. Soc.* **2001**, *123*, 11097−11098.
(50) van Beek, J. D.; Dupree, R.; Levitt, M. H. *J. Magn. Reson.* **2006**, *179*, 38−48.
(51) Gervais, C.; Dupree, R.; Pike, K. J.; Bonhomme, C.; Profeta, M.; Pickard, C. J.; Mauri, F. *J. Phys. Chem. A* **2005**, *109*, 6960−6969.
(52) Guerra, C. F.; Snijders, J. G.; te Velde, G.; Baerends, E. J. *Theor. Chem. Acc.* **1998**, *99*, 391−403.
(53) te Velde, G.; Bickelhaupt, F. M.; Baerends, E. J.; Guerra, C. F.; van Gisbergen, S. J. A.; Snijders, J. G.; Ziegler, T. *J. Comput. Chem.* **2001**, *22*, 931−967.
(54) ADF2005.01, SCM, Theoretical Chemistry, Vrije Universiteit, Amsterdam, The Netherlands, http://www.scm.com.
(55) Munowitz, M. G.; Griffin, R. G. *J. Chem. Phys.* **1982**, *76*, 2848−2858.
(56) Hahn, E. L. *Phys. Rev.* **1950**, *80*, 580−594.
(57) Lee, Y. K.; Kurur, N. D.; Helmle, M.; Johannessen, O. G.; Nielsen, N. C.; Levitt, M. H. *Chem. Phys. Lett.* **1995**, *242*, 304−309.
(58) Edén, M.; Levitt, M. H. *J. Chem. Phys.* **1999**, *111*, 1511−1519.
(59) Brinkmann, A.; Edén, M.; Levitt, M. H. *J. Chem. Phys.* **2000**, *112*, 8539−8554.
(60) Carravetta, M.; Edén, M.; Johannessen, O. G.; Luthman, H.; Verdegem, P. J. E.; Lugtenburg, J.; Sebald, A.; Levitt, M. H. *J. Am. Chem. Soc.* **2001**, *123*, 10628−10638.
(61) Brinkmann, A.; Edén, M. *J. Chem. Phys.* **2004**, *120*, 11726−11745.
(62) Edén, M. *Concepts Magn. Reson. Part A* **2003**, *17A*, 117−154.
(63) Haeberlen, U. High-Resolution NMR in Solids. Selective Averaging. In *Advances in Magnetic Resonance* Academic Press: New York, 1976; Supplement 1.
(64) Nielsen, N. C.; Bildsøe, H.; Jakobsen, H. J.; Levitt, M. H. *J. Chem. Phys.* **1994**, *101*, 1805−1812.

(65) Brinkmann, A.; Schmedt auf der Günne, J.; Levitt, M. H. *J. Magn. Reson.* **2002**, *156*, 79−96.

(66) Karlsson, T.; Popham, J. M.; Long, J. R.; Oyler, N.; Drobny, G. P. *J. Am. Chem. Soc.* **2003**, *125*, 7394−7407.

(67) Kristiansen, P. E.; Carravetta, M.; Lai, W. C.; Levitt, M. H. *Chem. Phys. Lett.* **2004**, *390*, 1−7.

(68) Levitt, M. H. Composite Pulses. In *Encyclopedia of Nuclear Magnetic Resonance*; Grant, D. M., Harris, R. K., Eds.; Wiley: Chichester, England, 1996; Vol. 2.

(69) Edén, M. *Chem. Phys. Lett.* **2003**, *378*, 55−64.

(70) Edén, M. *Chem. Phys. Lett.* **2002**, *366*, 469−476.

(71) Samoson, A.; Tuherm, T.; Gan, Z. *Solid State NMR* **2001**, *20*, 130−136.

(72) van Beek, J. D. MatNMR is a toolbox for processing NMR/EPR data under MATLAB and can be freely downloaded at http://matnmr.sourceforge.net.

(73) Bennett, A. E.; Rienstra, C. M.; Auger, M.; Lakshmi, K. V.; Griffin, R. G. *J. Chem. Phys.* **1995**, *103*, 6951−6958.

(74) Samoson, A. *Chem. Phys. Lett.* **1985**, *119*, 29−32.

(75) Cheng, V. B.; Henry, H.; Suzukawa, J.; Wolfsberg, M. *J. Chem. Phys.* **1973**, *59*, 3992−3999.

(76) Iuga, D.; Schäfer, H.; Verhagen, R.; Kentgens, A. P. M. *J. Magn. Reson.* **2000**, *147*, 192−209.

(77) Bak, M.; Nielsen, N. C. *J. Magn. Reson.* **2000**, *147*, 296−330.

(78) Frey, M. N.; Koetzle, T. F.; Lehmann, M. S.; Hamilton, W. C. *J. Chem. Phys.* **1973**, *58*, 2547−2556.

(79) Perdew, J. P.; Chevary, J. A.; Vosko, S. H.; Jackson, K. A.; Pederson, M. R.; Singh, D. J.; Fiolhais, C. *Phys. Rev. B* **1992**, *46*, 6671−6687.

(80) Becke, A. D. *Phys. Rev. A* **1988**, *38*, 3098−3100.

(81) Lee, C.; Yang, W.; Parr, R. G. *Phys. Rev. B* **1988**, *37*, 785−789.

(82) Sakellariou, D.; Hodgkinson, P.; Emsley, L. *Chem. Phys. Lett.* **1998**, *293*, 110−118.

(83) Williamson, P. T. F.; Verhoeven, A.; Ernst, M.; Meier, B. H. *J. Am. Chem. Soc.* **2003**, *125*, 2718−2722.

(84) Seber, G. A. F.; Wild, C. J. *Nonlinear Regression;* Wiley Series in Probability and Statistics; Wiley-Interscience: Hoboken, NJ, 2003.

(85) Ishii, Y.; Terao, T.; Hayashi, S. *J. Chem. Phys.* **1997**, *107*, 2760−2774.

(86) Case, D. A. *J. Biomol. NMR* **1999**, *15*, 95−102.

(87) Jaroniec, C. P.; Tounge, B. A.; Herzfeld, J.; Griffin, R. G. *J. Am. Chem. Soc.* **2001**, *123*, 3507−3519.

(88) Trebosc, J.; Amoureux, J. P.; Wiench, J. W.; Pruski, M. *Chem. Phys. Lett.* **2003**, *374*, 432−438.

(89) Levitt, M. H. *Spin Dynamics*: *Basic Principles of NMR Spectroscopy;* Wiley: Chichester, England, 2001.

(90) Markley, J. L.; Bax, A.; Arata, Y.; Hilbers, C. W.; Kaptein, R.; Sykes, B. D.; Wright, P. E.; Wüthrich, K. *Pure Appl. Chem.* **1998**, *70*, 117−142.